JOURNAL OF GUIDANCE, CONTROL, AND DYNAMICS
Vol. 15, No. 6, November-December 1992

Stochastic Measures of Performance Robustness in Aircraft Control Systems

Laura Ryan Ray*
Clemson University, Clemson, South Carolina 29634
and
Robert F. Stengel†
Princeton University, Princeton, New Jersey 08544

Stochastic robustness, a simple technique used to estimate the robustness of linear, time-invariant systems, is applied to a twin-jet transport aircraft control system. Concepts behind stochastic *stability* robustness are extended to stochastic *performance* robustness. Stochastic performance robustness measures based on classical design specifications and measures specific to aircraft handling qualities are introduced. Confidence intervals for comparing two control system designs are presented. The application of stochastic performance robustness, the use of confidence intervals, and tradeoffs between performance objectives are demonstrated by means of the twin-jet aircraft example.

Introduction

STANDARD linear control system design techniques rely on accurate models of the system to be controlled. Because models are never perfect, robustness analysis is necessary to determine the possibility of instability or inadequate performance in the face of uncertainty. Robustness to these uncertainties, parametric or unstructured, is normally treated deterministically and often without regard for possible physical variations in the system. Consequently, overconservative control system designs or designs that are insufficiently robust in the face of real-world uncertainties are a danger.

Stochastic robustness analysis (SRA), a simple technique to determine the robustness of linear, time-invariant systems by Monte Carlo methods, was introduced in Ref. 1 and presented in detail in Refs. 2 and 3. These references described stochastic stability robustness analysis and introduced the probability of instability as a scalar measure of stability robustness. Confidence intervals for the scalar probability of instability were presented, and the stochastic root locus, or probability density of the closed-loop eigenvalues, graphically portrayed robustness properties. Because it uses knowledge of the statistics of parameter variations directly, SRA provides an inherently precise yet simple characterization of robustness. The physical meaning behind the probability of instability is apparent, and overconservative or insufficiently robust designs can be avoided. Applications of SRA to full-state feedback aircraft control systems were described in Ref. 4. The results presented there illustrated the use of stochastic stability robustness techniques in comparing control system designs and in including finite-dimensional uncertain dynamics.

Concepts behind stochastic stability robustness can be extended to provide insight about control system design for performance. Design specifications such as rise time, overshoot, settling time, dead time, and steady-state error normally are used as indicators of adequate performance and lend themselves to the same kind of analysis as already described. Concepts of stochastic stability robustness analysis can be applied to these criteria giving probabilistic bounds on scalar performance criteria. Metrics resulting from SRA can be related to controller design parameters, thus providing a foundation for design tradeoffs and optimization. Extensions and uses of stochastic performance robustness in aircraft control system design and analysis are described in the following, and they are illustrated by means of an example.

Stochastic Performance Robustness

Stochastic stability robustness analysis is based on Monte Carlo analysis of the probability of instability P, and associated confidence intervals, given a statistical description of parameter uncertainty.[2-4] Because the stability test is binomial (i.e., the outcome of each Monte Carlo evaluation takes one of two values: stable or unstable), lower L and upper U confidence bounds are calculated using the binomial test.[5] While stability is an important element of robustness, performance robustness analysis is vital to determining whether important design specifications are met. Adequate performance, such as initial condition response, command response, control authority, and rejection of disturbances, is difficult to describe by a single scalar metric. Nevertheless, elements of stochastic stability robustness analysis apply for binomial performance metrics.

Numerous criteria stemming from classical control concepts exist as measures of adequate performance. Appealing to these, one can begin a smooth transition from stability robustness analysis to performance robustness analysis simply by analyzing the degree of stability or instability rather than strict stability. As described in Ref. 2, one method of doing this is to shift the vertical discriminant line from zero to $\Sigma <$ (or $>$) 0. Histograms and cumulative distributions for varying degrees of stability are readily given by the Monte Carlo estimate of the probability of any eigenvalue real-part exceeding Σ. Binomial confidence intervals are applicable to each point of the cumulative distribution as there are just two values of interest, e.g., satisfactory or unsatisfactory. P is a special case where $\Sigma = 0$. The robustness metric resulting from the cumulative probability distribution is directly related to classical concepts of rates of decay (growth) of first- and second-order closed-loop responses, time-to-half, and time-to-double. Taking degree-of-stability analysis further, rather than a vertical discriminant line, one can confine the closed-loop roots to sectors in the complex plane bounded by lines of constant damping and arcs of constant natural frequency.[6] Systems with roots

Presented as Paper 90-3410 at the AIAA Guidance, Navigation, and Control Conference, Portland, OR, Aug. 20-22, 1990; received Feb. 25, 1991; revision received Dec. 16, 1991; accepted for publication Jan. 2, 1992.

*Assistant Professor, Department of Mechanical Engineering. Member AIAA.

†Professor, Department of Mechanical and Aerospace Engineering. Associate Fellow AIAA.

confined to these regions would be expected to display a certain transient response speed. Again, the probability of roots lying within a sector follows a binomial distribution, and binomial confidence intervals apply.

Performance specifications for aircraft flying qualities are detailed in Ref. 7 in terms of longitudinal and lateral-directional criteria at three levels of performance for each flight phase. Many flying-qualities criteria require little computation above and beyond eigenvalue computation, making performance robustness as easy to characterize as stability robustness. For example, the short-period response can be characterized by its damping ratio and natural frequency vs normal acceleration sensitivity to angle-of-attack n_α. The latter is illustrated in Ref. 7 by plotting the short-period undamped natural frequency vs n_α, as shown in Fig. 1. n_α is simply a function of the dynamic pressure $\bar{q}$ and vehicle parameters

$$n_\alpha \simeq \frac{\bar{q} S_{\text{ref}}}{mg} C_{L_\alpha} \tag{1}$$

C_{L_α} is the lift-curve slope, S_{ref} the wing reference area, m the mass, and g the gravitational constant. Short-period-mode requirement levels for each flight phase are characterized by calculating the closed-loop eigenvalues and evaluating Eq. 1. Repeated evaluations using Monte Carlo analysis give a distribution that can be shown pictorially on Fig. 1; the resulting measure of performance robustness is the probability of remaining within level 1, 2, or 3 criteria.[7] Binomial confidence interval computations can be applied to the scalar probability estimate.

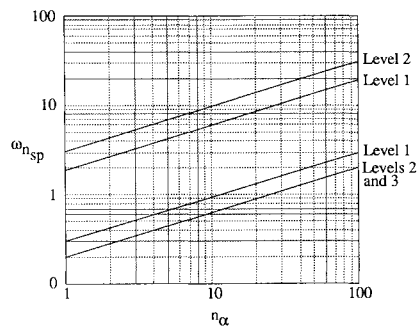

Fig. 1 Short-period response as characterized by n_α vs $\omega_{n_{sp}}$ for category B flight phase (climb, cruise, descent) and all aircraft classes.[7]

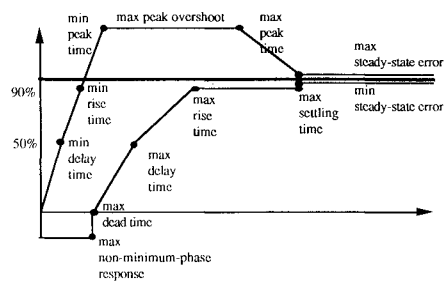

Fig. 2 Example of step response bounds formed by scalar performance characteristics.

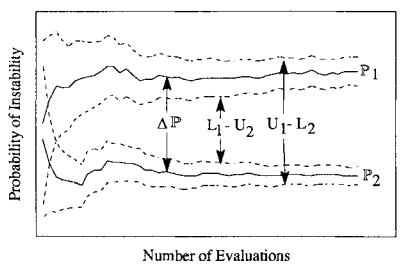

Fig. 3 Confidence interval calculation on the difference ΔP between two probabilities P_1 and P_2.

Table 1 Longitudinal parameters of the twin-jet aircraft

Uniform variation[a]	Description
15	Mass, slugs
15	Moment of inertia about the y axis, slug-ft^2
2	Wing reference area, ft
2	Aerodynamic chord, ft
2	Wing span, ft
30	Center-of-gravity location as a percent of mean aerodynamic chord
25	Lift-curve slope
25	Lift-curve intercept
40	Deviation of the basic lift coefficient due to Mach effects on lift-curve intercept
40	Deviation of the basic lift coefficient due to Mach effects on lift-curve slope
5	Variation in lift coefficient with rate of change of nondimensional α
7.5	Variation in lift coefficient with rate of change of nondimensional q
10	Variation in lift coefficient with change in elevator angle
50	Basic low-speed drag coefficient
25	Moment-curve slope
25	Moment-curve intercept
25	Deviation of the basic moment coefficient due to Mach effects on moment-curve intercept
10	Deviation in the basic moment coefficient due to Mach effects on moment-curve slope
10	Variation in moment coefficient with rate of change of nondimensional α
10	Variation in lift coefficient with rate of change of nondimensional q
15	Variation in moment coefficient with change in elevator angle
10	Center-of-gravity variation factor

[a] ± percent of nominal parameter value

Time responses provide the most clear-cut means of evaluating performance. Stochastic performance robustness can be portrayed as a distribution of possible trajectories around a nominal or desired trajectory. After defining "envelopes" around the nominal trajectory (Fig. 2), the probability of violating the envelopes can be computed using Monte Carlo evaluation. The envelope chosen around the nominal trajectory encompasses scalar performance measures; the trajectories in Fig. 2 are examples of bounds defined by minimum and/or maximum allowable dead time, delay time, rise time, time-to-peak overshoot, peak overshoot, settling time, and steady-state error.[6] Although it is simple to conclude that a response violates an envelope, individual responses within the envelope may not be acceptable. In such cases, the derivative of a response and envelopes around the derivative also can be used as performance criteria.[3]

The criteria defining envelopes that bound an acceptable time response are not unique; the segmented envelopes in Fig. 2 can be smoothed, or other scalars can be used to define points on the envelope. However, once an envelope is defined, time response distributions due to a command input, disturbance, initial condition, or some combination can be computed by Monte Carlo methods. For each evaluation, the trajectory is a binomial variable; it either stays within the envelope or violates the envelope, and binomial confidence intervals apply. Although individual time responses require more computation time than do individual sets of eigenvalues, such analysis is well within the capability of existing workstations.

Confidence intervals for the difference between two probabilities are useful when comparing two control system designs. A statistic on the difference decides whether one controller is more robust than another, either as part of an iterative design process or as imbedded in an optimization technique. The

Table 2 Scalar performance criteria defining command response envelope

Scalar metric	Value
Maximum dead time	2.5 s
Maximum nonminimum-phase response	−0.1 of desired steady-state value
Minimum and maximum delay time	1.0 s and 7.5 s
Minimum and maximum rise time	2.0 s and 15.0 s
Minimum and maximum peak time	3.0 s and 18.0 s
Maximum peak overshoot	1.25 of desired steady-state value
Maximum settling time	22.0 s
Minimum and maximum steady-state error	±0.025 of desired steady-state value

Table 3 Setpoint for individual velocity and flight-path-angle commands

Command	δT, %	δE, deg	V, fps	γ, deg	q, rad/s	α, deg
V = 15 fps	1.1	15.3	15	0	0	−0.25
γ = 4 deg	24.1	0.6	0	4	0	−0.01

statistics literature gives several methods of computing the confidence interval for the difference between two binomial variables. Reference 8 presents a method based solely on individual confidence intervals. Given individual intervals based on independent Monte Carlo trials,

$$\Pr(L_1 \le P_1 \le U_1) = 1 - \alpha_1 \tag{2}$$

$$\Pr(L_2 \le P_2 \le U_2) = 1 - \alpha_2 \tag{3}$$

the confidence interval around $\Delta P \triangleq P_1 - P_2$ is given by [8]

$$\Pr[(L_1 - U_2) \le \Delta P \le (U_1 - L_2)]$$

$$\ge 1 - \alpha_1 - \alpha_2 + \alpha_1\alpha_2 \tag{4}$$

When identical parameter sets are used to generate individual intervals, the right-hand side of Eq. (4) is $1 - \alpha_1 - \alpha_2$. Since (L_1, U_1) and (L_2, U_2) are computed using the binomial test and represent exact intervals for the individual estimates, Eq. (4) is not an approximation. Confidence interval comparisons are illustrated schematically in Fig. 3. The interpretation of the confidence interval for the difference is straightforward; the probability that the true difference lies within $[(L_1 - U_2), (U_1 - L_2)]$ is at least $1 - \alpha_1 - \alpha_2 + \alpha_1\alpha_2$. If the interval on ΔP contains zero (i.e., if the individual intervals overlap as they do initially in Fig. 3), then the difference in robustness between the two systems is not proven significant at that number of evaluations. If the true difference ΔP is small, a larger number of evaluations may result in an interval that does not contain zero, as in Fig. 3.

A given ΔP can result from many combinations of individual probability estimates, and it is difficult to generalize the number of evaluations necessary to detect a difference of a certain magnitude. Nevertheless, the number of evaluations required for an individual confidence interval can be used to foretell the number of evaluations necessary to detect a difference between two estimates. Figure 4 gives the required number of evaluations J for each individual confidence interval, for the special case, $\alpha_1 = \alpha_2 = 0.05$. Using the difference $P_2 - P_1$ as the ordinate and P_1 as the abscissa, the curves show the minimum number of evaluations required to establish a significant difference. For example, if the probability estimates (denoted $\hat{P}$) are $\hat{P}_2 = 0.45$ and $\hat{P}_1 = 0.4$, Fig. 4 shows that a statistically significant difference (i.e., nonoverlapping confidence intervals) can be determined using approximately 1500 Monte Carlo evaluations. Individual estimates of $\hat{P}_2 = 0.15$ and $\hat{P}_1 = 0.1$ result in the same difference, but fewer than 750 evaluations are required to detect the difference. Figure 4 is based on individual confidence interval calculations, as presented in Ref. 3.

Performance Robustness of Longitudinal Controllers For a Jet Transport

SRA is applied to a twin-jet transport aircraft, with the goal of characterizing the performance robustness of longitudinal

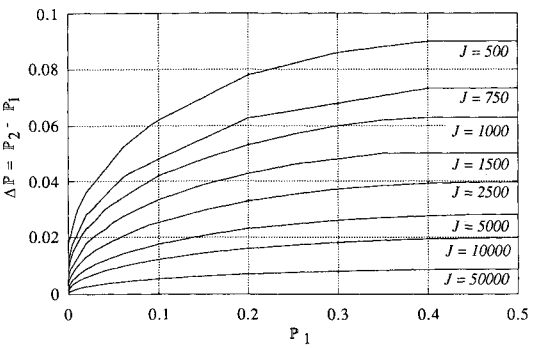

Fig. 4 Number of evaluations establishing significant differences between two probabilities for 95% confidence intervals and equal numbers of evaluations for individual probabilities.

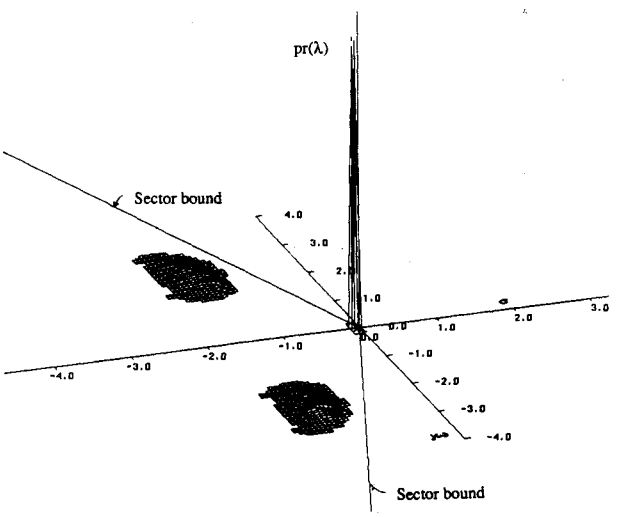

a) Stochastic root locus with sector bounds defined by minimum level 1 short-period damping for cruise flight

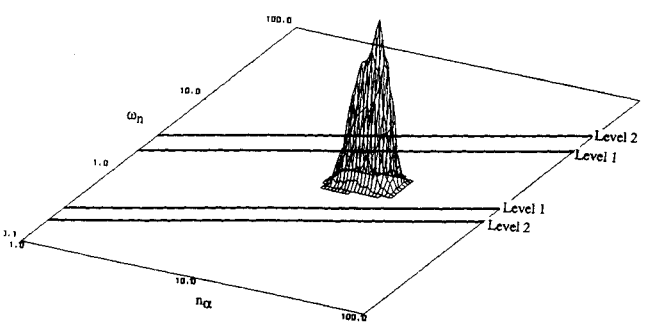

b) Short-period frequency vs acceleration sensitivity distribution

Fig. 5 Stochastic robustness evaluation of the open-loop short-period dynamics of the twin-jet aircraft, based on 10,000 Monte Carlo evaluations.

command responses. The rigid-body nonlinear longitudinal equations are

$$\begin{bmatrix} \dot{V} \\ \dot{\gamma} \\ \dot{q} \\ \dot{\alpha} \end{bmatrix} = \begin{bmatrix} \dfrac{-D + T\cos(\alpha)}{m} - g\sin(\gamma) \\ \dfrac{L + T\cos(\alpha)}{mV} - \dfrac{g\cos(\gamma)}{V} \\ \dfrac{M}{I_{yy}} \\ q - \dot{\gamma} \end{bmatrix} \tag{5}$$

where $[V, \gamma, q, \alpha]$ represent velocity, flight-path-angle, pitch rate, and angle-of-attack, $[L, D, M]$ are aerodynamic lift, drag, and pitching moment, T is the thrust, and g is the gravitational constant. Equation (5) depends on a number of parameters given in Table 1. Mean parameter values of the stability derivatives in Table 1 are functions of Mach number and altitude; they are interpolated from aerodynamic data curves for the aircraft at a given trim condition.[9] The aerodynamic model used to compute L, D, and M is a simplified version of that given in Ref. 9, modified to use only two longitudinal controls (thrust and elevator). In this example, each Monte Carlo evaluation begins with the nonlinear equations of motion and associated parameters. The nonlinear equations are evaluated using appropriately distributed random parameters and are then linearized around the nominal trim condition. The closed-loop eigenvalues and performance metrics are evaluated from the linearized system.

The parameters are assumed to have uniform variations of the magnitudes given in Table 1. For the wing parameters (S_{ref}, chord, span), these variations are representative of loose manufacturing tolerances. The mass and moment-of-inertia variations are based on the maximum and minimum possible values of these parameters given in Ref. 9. The remaining parameter-variation estimates are based on interpolation accuracy and possible flight condition variations around the nominal value.

Trim conditions for a flight condition of $V = 425$ fps (130 m/s) at an altitude of 5000 ft (1524 m) are as follows: thrust = 27.3%, elevator = −0.65 deg, and angle-of-attack = 2.15 deg. The open-loop eigenvalues for the state matrix resulting from linearizing Eq. (5) around trim are $\lambda = -1.32 \pm 2.44j$, $-0.0053 \pm 0.0962j$. Stochastic robustness evaluation using the short-period Mil-spec requirements[7] shows an acceptable open-loop short-period mode for the uniform parameter variations given in Table 1. Figure 5a shows the stochastic root locus with sectors defined by minimum level 1 short-period damping ratio for cruise or climb (category B flight phase); for 10,000 evaluations, the short-period eigenvalues never violate the level 1 damping restriction. Figure 5b characterizes the short-period frequency vs acceleration sensitivity, which also remains within level 1 constraints for 10,000 evaluations. The probability estimate of violating level 1 short-period specifications is 0, with 95% confidence intervals of (0, 3.69E − 4).

Design of Longitudinal Controllers

A command response that stays within the envelope described by scalar criteria in Table 2 serves as the performance requirement for designing linear regulators for velocity and flight-path-angle commands. In addition, elevator deflections are limited to ±30 deg, and thrust commands must remain between 0 and 100%. The desired commands $y^* = V^*$ or $y^* = \gamma^*$ and corresponding setpoints $\mathbf{x}^* = [V\ \gamma\ q\ \alpha]^T$, $\mathbf{u}^* = [\delta T\ \delta E]$ are given in Table 3. The open-loop responses to individual velocity and flight-path-angle commands are inadequate because of the slow, lightly damped phugoid mode. Numerical values of the results that follow depend heavily on the performance criteria chosen. The envelopes defined in Table 2 reflect tolerable variations around an acceptable nominal response. The control limits are typical of those for a jet transport. Changing the time response envelopes or control authority limits would give different numerical results. The emphasis in this example is not on the specific criteria chosen, but on how SRA characterizes performance given a control system design and performance specifications.

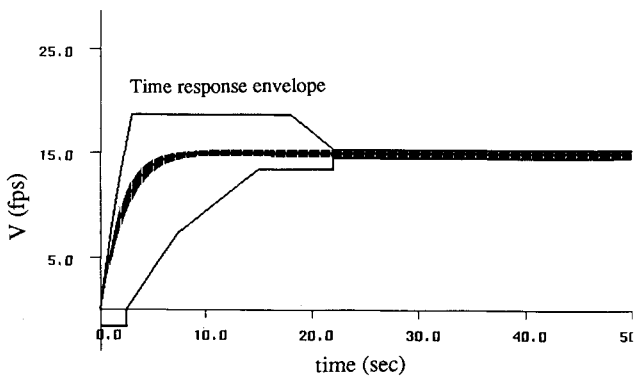

a) 15 fps velocity command: velocity response

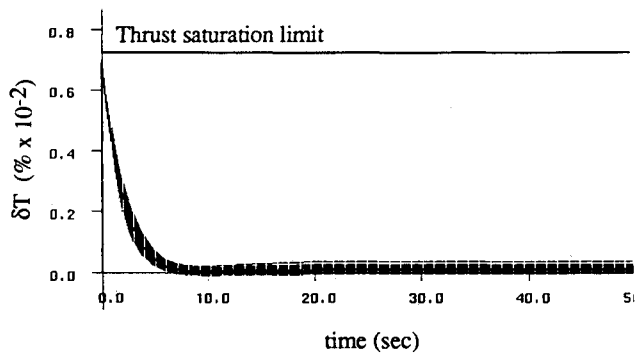

b) 15 fps velocity command: thrust response

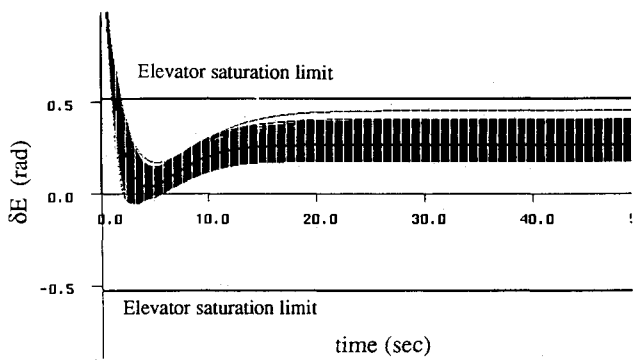

c) 15 fps velocity command: elevator response

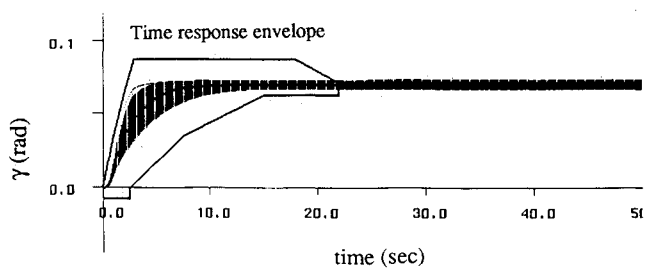

d) 4-deg flight-path-angle command: flight-path-angle response

Fig. 6 Closed-loop command responses using IMF controller, 500 Monte Carlo evaluations. Nominal response is indicated by the solid line.

Structured linear-quadratic regulators[10] offer a simple means of designing a linear control system with desirable performance and robustness characteristics. Specifications of the linear-quadratic performance index and subsequent control gains using implicit-model-following (IMF) minimizes the dynamic response error between the closed-loop system and an ideal model.[10] State, control, and cross-weighting matrices (**Q**, **R**, **M**) are based on a quadratic cost function that weights the difference between the actual state rate ($\dot{\mathbf{x}}$) and that of an ideal model ($\dot{\mathbf{x}}_M$), where

$$\dot{\mathbf{x}}_M = \mathbf{F}_M \mathbf{x}_M \tag{6}$$

IMF offers a straightforward way of designing controllers that approximate desired dynamic characteristics. For this example, the ideal model was chosen to increase the natural frequency and damping of the phugoid mode, while maintaining acceptable short period response:

$$\mathbf{F}_M = \begin{bmatrix} -0.3 & -32.17 & -0.0104 & -23.34 \\ 0.00381 & -0.1949 & 0.0006 & 1.356 \\ 0.0 & -0.0 & -1.273 & -5.981 \\ -0.0038 & 0.1949 & 0.999 & -1.356 \end{bmatrix} \tag{7}$$

$$\gamma_M = \begin{cases} -1.35 \pm 2.39j \\ -0.213 \pm 0.314j \end{cases} \tag{8}$$

Stochastic performance robustness analysis is based on the probability of violating the desired time response envelopes ($\hat{P}_V$ and $\hat{P}_\gamma$) and the probability of control saturation ($\hat{P}_{\delta T}$ and $\hat{P}_{\delta E}$).

The IMF controller gives a nominal closed-loop command response to separate velocity (Figs. 6a–c) and flight-path-angle (Fig. 6d) commands that is within the acceptable time-response envelope. Figure 6 also shows 500 Monte Carlo evaluations of the command response; the nominal steady-state control inputs and state are given in Table 3, and the nominal response in Fig. 6 is indicated by a solid line. The response and associated envelopes in Fig. 6 are shown for the commanded variable only; the remaining state elements do not require performance constraints in this example. Thrust and elevator time histories are shown for the velocity command response only. Parameter uncertainty effects appear as variations around the nominal response, indicated by the dark distribution and associated outliers. Parameter uncertainty results in a distribution of transient responses that stays within the envelope, and nonzero steady-state errors that violate the envelope for both velocity (Fig. 6a) and flight-path-angle (Fig. 6d) commands. Based on 500 Monte Carlo time response evaluations, the estimate $\hat{P}_V$ is 0.002 with 95% confidence intervals (5.1E − 5, 0.0111) and the estimate $\hat{P}_\gamma$ is 0.368 (0.326, 0.412). The nominal elevator response violates control limits for both command responses, and in each case, the probability of elevator saturation is $\hat{P}_{\delta E} = 1.0$. Note that the control saturation limits in Figs. 6b–c are adjusted to reflect the remaining control authority after considering trim requirements.

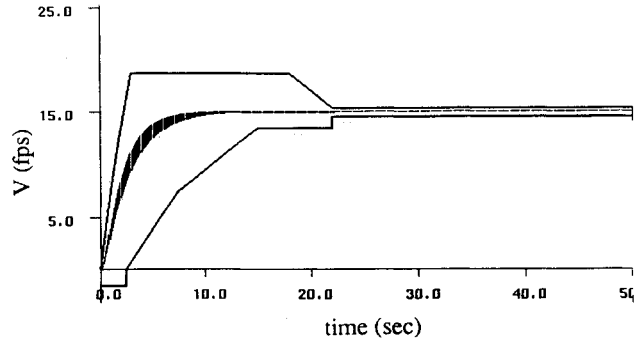

a) 15 fps velocity command: velocity response

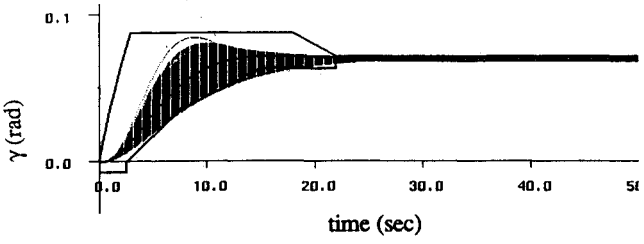

d) 4-deg flight-path-angle command: flight-path-angle response

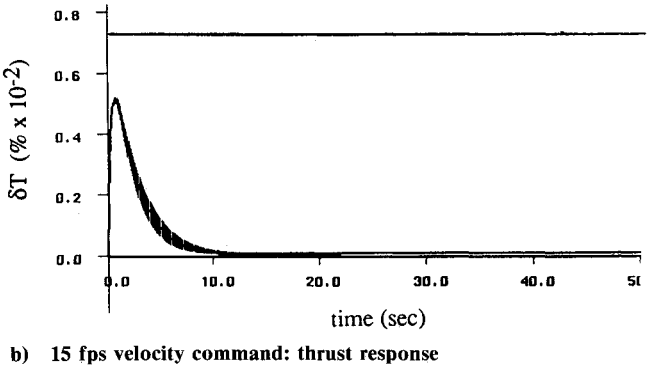

b) 15 fps velocity command: thrust response

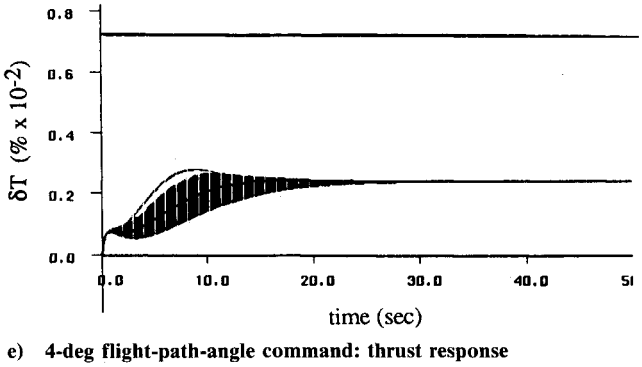

e) 4-deg flight-path-angle command: thrust response

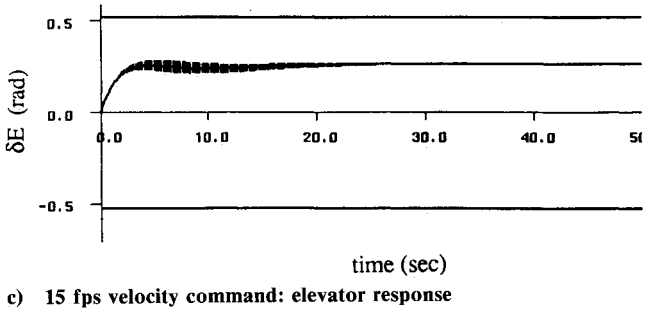

c) 15 fps velocity command: elevator response

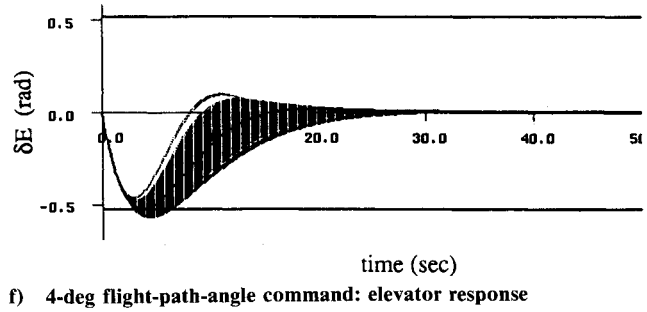

f) 4-deg flight-path-angle command: elevator response

Fig. 7 Closed-loop command response using PFIMF controller, with filter control weighting $\mathbf{R}_F$ = diag(10, 50), 500 Monte Carlo evaluations. Nominal response is indicated by the solid line.

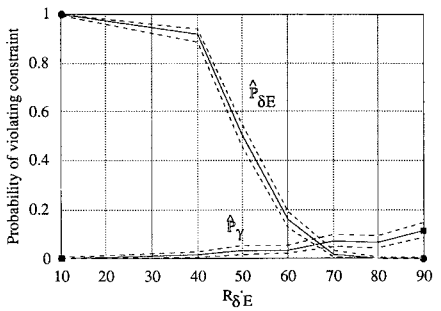

Fig. 8 Stochastic performance robustness evaluation with PFIMF: Probability of violating flight-path-angle command response $\hat{P}_\gamma$ and probability of violating elevator saturation limits $\hat{P}_{\delta E}$ vs filter weight $R_{\delta E}$. Solid lines give probability estimates, dashed lines give confidence intervals.

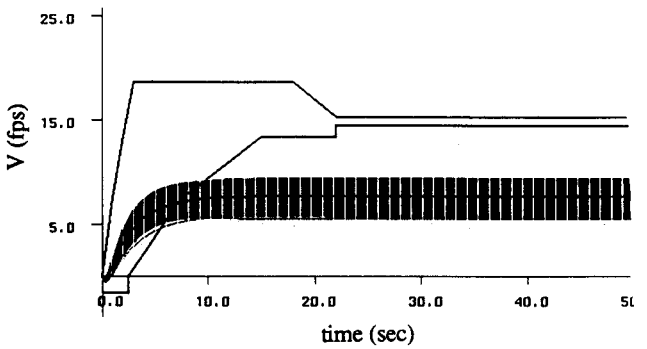

Fig. 9 Closed-loop command response using PFIMF controller, with filter control weighting $\mathbf{R}_F = \text{diag}(10, 50)$, 500 Monte Carlo evaluations: 15 fps velocity command subject to constant disturbance $w_v = 40$ fps. Nominal response is indicated by the solid line.

Implicit model following modified by state augmentation[10] can help meet control authority constraints. Proportional-filter (PF) compensation adds integrators to restrict the control rates, thus preventing instantaneous control changes and reducing the maximum control effort. The control vector is appended to the state vector

$$\begin{bmatrix} \dot{\tilde{\mathbf{x}}} \\ \dot{\tilde{\mathbf{u}}} \end{bmatrix} = \begin{bmatrix} \mathbf{F} & \mathbf{G} \\ \mathbf{0} & \mathbf{0} \end{bmatrix} \begin{bmatrix} \tilde{\mathbf{x}} \\ \tilde{\mathbf{u}} \end{bmatrix} + \begin{bmatrix} \mathbf{0} \\ \mathbf{I} \end{bmatrix} v(t) \tag{9}$$

where $\mathbf{F}$ and $\mathbf{G}$ are the nominal dynamic and control effect matrices, $\tilde{\mathbf{x}} = \mathbf{x}(t) - \mathbf{x}^*$, $\tilde{\mathbf{u}} = \mathbf{u}(t) - \mathbf{u}^*$, and $v(t)$ is a commanded control rate. The PFIMF state weighting matrix is

$$\mathbf{Q}_F = \begin{bmatrix} \mathbf{Q} & \mathbf{M} \\ \mathbf{M}^T & \mathbf{R} \end{bmatrix} \tag{10}$$

where $\mathbf{Q}$, $\mathbf{R}$, $\mathbf{M}$ are the original (IMF) weighting matrices. A weighting matrix, $\mathbf{R}_F$, constrains the control rates. Elements of $\mathbf{R}_F$ affect the bandwidth of each control; the larger the weight, the more the control rate is restricted.

The IMF regulator is augmented to include low-pass filtering of the control command, with a diagonal control-rate weighting matrix $\mathbf{R}_F = \text{diag}[10, 50]$. Figure 7 shows 500 stochastic state and control histories to individual velocity and flight-path-angle commands using the PFIMF controller and a stream of random numbers independent from the IMF case. The (1, 1) element of $\mathbf{R}_F$ ($R_{\delta T}$) determines the amount of filtering on thrust rate, and the (2, 2) element ($R_{\delta E}$) controls elevator rate. With filter elements, the control rates are no longer unlimited, and the mean control responses remain unsaturated. Steady-state error due to parameter uncertainty remains within the desired state history envelope for the velocity command response (Fig. 7a). Steady-state error for the γ command improves, although the variation in the γ transient response is much greater than that of the IMF regulator alone, as seen by comparing Figs. 6d and 7d. $\hat{P}_V$ and $\hat{P}_\gamma$ estimates corresponding to Fig. 7 are 0.0 (0.0, 0.0074) and 0.034 (0.0199, 0.0539), respectively. For 500 evaluations, the PFIMF flight-path-angle command response improvement over the IMF case alone proves significant by application of confidence intervals on the difference $(P_{\gamma_{\text{IMF}}} - P_{\gamma_{\text{PFIMF}}})$. Applying Eq. 4,

$$\Pr[0.2721 \le (P_{\gamma_{\text{IMF}}} - P_{\gamma_{\text{PFIMF}}}) \le 0.3921] \ge 0.9025 \tag{11}$$

Equation 11 states that with PF augmentation between 27 and 39%, more of the flight-path-angle responses lie within the envelope, with a confidence coefficient of at least 0.9025. The mean elevator response for the flight-path-angle command dips just to saturation limits, and the probability of elevator saturation is $\hat{P}_{\delta E_{\text{PFIMF}}} = 0.502$ (0.457, 0.547).

Stochastic robustness analysis shows that PF augmentation improves performance objectives by reducing control rates and steady-state error due to uncertainty. The state and control response to the velocity command prove acceptable ($\hat{P}_V$, $P_{\delta E}$, and $\hat{P}_{\delta T}$ all equal 0), and the improved responses to flight-path-angle command are statistically significant. For the flight-path-angle command, SRA demonstrates the tradeoff between the two performance objectives; increasing the (2, 2) element ($R_{\delta E}$) of $\mathbf{R}_F$ will further reduce elevator command authority at the expense of the γ time response. Figure 8 illustrates this tradeoff by showing $\hat{P}_\gamma$, $\hat{P}_{\delta E}$, and their confi-

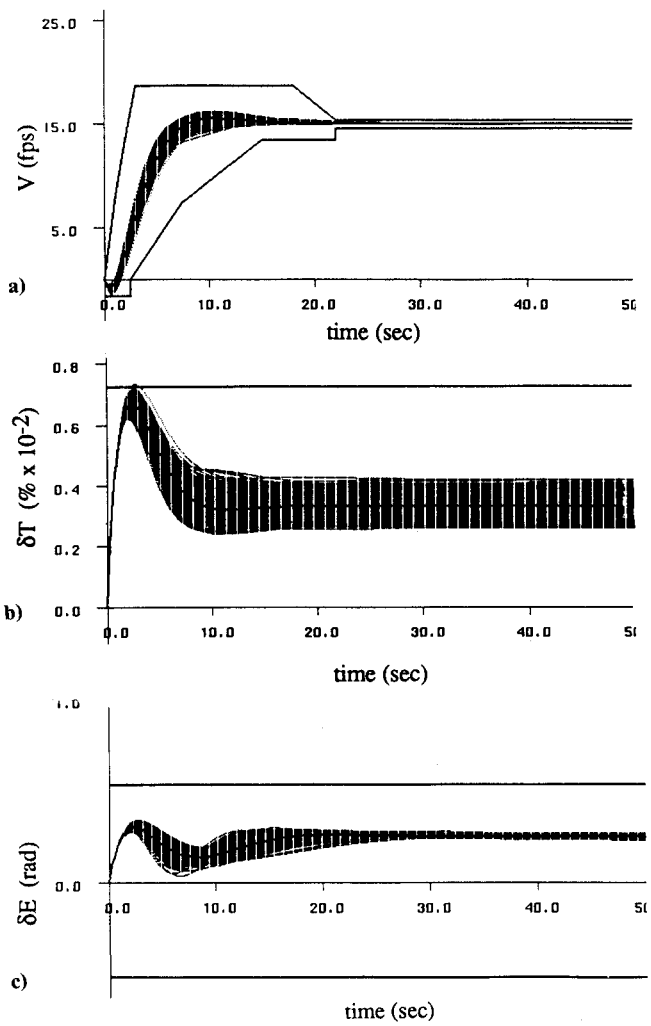

Fig. 10 Closed-loop command response using PIFIMF controller, with filter control weighting $\mathbf{R}_F = \text{diag}(200, 50)$, and integral state weighting $\mathbf{Q}_I = \text{diag}(0.1, 100)$, 500 Monte Carlo evaluations: 15 fps velocity command subject to constant disturbance $w_v = 40$ fps. Nominal response is indicated by the solid line.

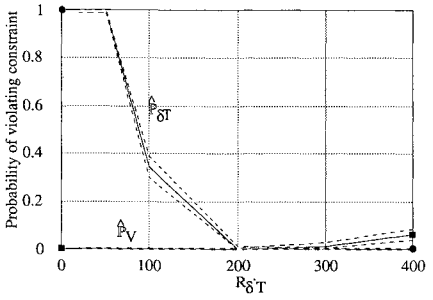

Fig. 11 Stochastic performance robustness evaluation with PIFIMF: Probability of violating velocity command response envelope $\hat{P}_V$ and probability of violating thrust saturation limits $\hat{P}_{\delta T}$ vs filter weight $R_{\dot{\delta}T}$. Solid lines give probability estimates, dashed lines give confidence intervals.

dence intervals as functions of the design parameter $R_{\dot{\delta}E}$. A plot like Fig. 8 can be used to choose the filter weight that gives the smallest probabilities of envelope violation while adhering as well as possible to the control authority restrictions. In this case, it is not possible to simultaneously reduce $\hat{P}_\gamma$ and $\hat{P}_{\delta E}$ to zero by varying $R_{\dot{\delta}E}$. Nevertheless, stochastic robustness analysis offers a simple, understandable means of relating design parameters to performance objectives and of choosing the best control gains to meet those objectives.

Design of a Longitudinal Controller for Disturbance Rejection

As a final example, the preceding analysis is extended to encompass a performance constraint on disturbance rejection. The equations of motion are modified to include a vertical wind disturbance w_v

$$\begin{bmatrix} \dot{V} \\ \dot{\gamma} \end{bmatrix} = \begin{bmatrix} \dfrac{-D\sin(\alpha-\alpha_a)+T\cos(\alpha-\alpha_a)}{m} - g\sin(\gamma) \\ \dfrac{L\sin(\alpha-\alpha_a)+T\cos(\alpha-\alpha_a)}{mV} - \dfrac{g\cos(\gamma)}{V} \end{bmatrix} \tag{12}$$

where

$$\alpha_a = \alpha + \gamma - \tan^{-1}\frac{V\sin(\gamma)+w_v}{V\cos(\gamma)} \tag{13}$$

With the disturbance present, the state components represent inertial velocity, flight-path-angle, pitch, and angle-of-attack, and the disturbance enters through the expression for air-relative angle-of-attack α_a. A disturbance input matrix is defined for robustness analysis by numerical linearization of the nonlinear equations with respect to w_v, around the nominal condition $w_v = 0$. Velocity command response subject to a constant 40-fps vertical velocity disturbance using the PFIMF controller is shown in Fig. 9. The mean response shows a nonzero steady-state error that violates the command response envelope, and uncertainty causes a larger spread around the nominal response than that of the system without the disturbance (Fig. 7). Also, the steady-state flight-path-angle (not shown) is less than zero due to the disturbance.

Proportional-integral (PI) compensation introduces a command-error integral for each commanded state element, zeroing steady-state error and improving disturbance rejection characteristics. The perturbation equations for the nominal system are

$$\begin{bmatrix} \dot{\tilde{\mathbf{x}}} \\ \dot{\xi} \end{bmatrix} = \begin{bmatrix} \mathbf{F} & \mathbf{0} \\ \mathbf{H} & \mathbf{0} \end{bmatrix} \begin{bmatrix} \tilde{\mathbf{x}}(t) \\ \xi(t) \end{bmatrix} + \begin{bmatrix} \mathbf{G} \\ \mathbf{0} \end{bmatrix} \tilde{\mathbf{u}}(t) \tag{14}$$

$$\mathbf{H} = \begin{bmatrix} 1 & 0 & 0 & 0 \\ 0 & 1 & 0 & 0 \end{bmatrix} \tag{15}$$

where

$$\xi(t) = \xi(0) + \int_0^t \tilde{\mathbf{y}}(\tau)\,d\tau \tag{16}$$

and $\tilde{\mathbf{y}}(t) = \mathbf{y}(t) - \mathbf{y}^*$. Here, $\mathbf{y}^* = [V\ \gamma]^T$, and a (2×2) weighting matrix $\mathbf{Q}_I$ is appended to the original state weighting matrix. Diagonal elements of $\mathbf{Q}_I$ affect the rate at which the command error integrals approach zero. The diagonal components are chosen to keep the velocity command within the desired envelope and to zero the flight-path-angle response. Command error integrals are added to the existing PFIMF controller, and for the resulting PIFIMF system with $\mathbf{Q}_I = \text{diag}[0.01, 100]$ and $\mathbf{R}_F = \text{diag}[200, 50]$, Fig. 10 shows an improved velocity command response $\mathbf{y}^* = [V^*\ 0]^T$. The 500-evaluation probability estimates and 95% confidence intervals are $\hat{P}_V = 0$ (0.0, 7.4E-3) and $\hat{P}_{\delta T} = 0.002$ (5.1E-5, 0.0111). The (1, 1) component of $\mathbf{R}_F$ is increased to restrain thrust as the command error integrals are introduced. Figure 11 shows analysis of the tradeoff between $\hat{P}_V$ and $\hat{P}_{\delta T}$ as a function of design parameter $R_{\dot{\delta}T}$ comparable to that presented for the flight-path-angle response in Fig. 8. Again, Fig. 11 can be used to choose control system design parameters that best meet performance objectives.

Conclusion

Stochastic robustness analysis offers a rigorous yet straightforward alternative to other robustness metrics that is simple to compute and is unfettered by normally difficult problem statements, such as non-Gaussian statistics, products of parameter variations, and structured uncertainty. The analysis embraces both stability and performance metrics, handling qualities requirements, and more general responses. Binomial confidence intervals provide statistical bounds on the probability of instability and on performance metrics. Statistical comparisons of control system robustness also are rendered through confidence intervals. Both stability and performance metrics resulting from stochastic robustness analysis provide details relating system specifications intrinsic to a given application and control system design parameters. Stochastic robustness analysis has a significant role to play in computer-aided control system design.

Acknowledgments

This research has been sponsored by the Federal Aviation Administration and the NASA Langley Research Center under Grant No. NGL 31-001-252 and by the Army Research Office under Grant No. DAAL03-89-K-0092.

References

[1]Stengel, R. F., "Some Effects of Parameter Variations on the Lateral-Directional Stability of Aircraft," *Journal of Guidance and Control,* Vol. 3, No. 2, 1980, pp. 124-131.

[2]Stengel, R. F., and Ray, L. R., "Stochastic Robustness of Linear Time-Invariant Control Systems," *IEEE Transactions on Automatic Control,* Vol. 36, No. 1, 1991, pp. 82-87.

[3]Ray, L. R., *Stochastic Robustness of Linear Multivariable Control Systems: Towards Comprehensive Robustness Analysis,* Ph.D. Dissertation, Dept. of Mechanical and Aerospace Engineering, Princeton Univ., MAE-1902-T, Princeton, NJ, 1991.

[4]Ray, L. R., and Stengel, R. F., "Application of Stochastic Robustness to Aircraft Control Systems," *Journal of Guidance, Control, and Dynamics,* Vol. 14, No. 6, 1991, pp. 1251-1259.

[5]Conover, W. J., *Practical Non-Parametric Statistics,* Wiley, New York, 1980.

[6]Franklin, G. F., et al., *Feedback Control of Dynamic Systems,* Addison-Wesley, Reading, MA, 1991.

[7]*Military Specification Flying Qualities of Piloted Airplanes,* U.S. Air Force, MIL-F-8785C, Wright-Patterson AFB, OH, Nov. 1980.

[8]Lavenberg, S. S., (ed.), *Computer Performance Modeling Handbook,* Academic, New York, 1983.

[9]*TVC Simulation Engineering Manual,* Boeing Co., Jan. 1982.

[10]Stengel, R. F., *Stochastic Optimal Control: Theory and Application,* Wiley, New York, 1986, Chap. 6.